

Two-color QCD in a strong magnetic field: The role of the Polyakov loop

Arturo Amador* and Jens O. Andersen†

Department of Physics, Norwegian University of Science and Technology, Høgskoleringen 5, N-7491 Trondheim, Norway

(Dated: October 13, 2018)

We study two-color QCD in a constant external magnetic background at finite temperature using the Polyakov-loop extended two-flavor two-color NJL model. At $T = 0$, the chiral condensate is calculated and it is found to increase as a function of the magnetic field B . In the chiral limit the deconfinement transition lies below the chiral transition for nonzero magnetic fields B . At the physical point, the two transitions seem to coincide for field strengths up to $|qB| \approx 5M_\pi^2$, where $M_\pi = 140$ MeV, whereafter they split, and the deconfinement transition takes place first. The splitting between the two increases as a function of B in both the chiral limit and at the physical point. At the physical point, the transition temperature decreases slightly for magnetic fields up to $|qB| \approx 3M_\pi^2$, whereafter it increases monotonically. In the chiral limit, this behavior is less pronounced. This change of slope is absent in the NJL model where T_c increases for all values of $|qB|$. In the range from zero magnetic field and $|qB| = 20M_\pi^2$, the transition temperature for the chiral transition increases by approximately 35 MeV, while the transition temperature for deconfinement is essentially constant.

PACS numbers:

I. INTRODUCTION

The behavior of hadronic matter at finite temperature and density in strong external magnetic fields has received a lot of attention for many years, see for example Ref. [1] for a very recent review. The problem of strongly interacting matter in a strong magnetic background arises in various contexts. For example, magnetars, which are a certain type of neutron stars, have very strong magnetic fields of the order of 10^{10} Tesla (T) [2]. Some of the properties of stars such as the mass-radius relation are determined by the equation of state. The determination of the bulk properties of a Fermi gas in an external magnetic field is therefore important for the understanding of these compact stellar objects. Similarly, large magnetic fields, up to the order of $eB \sim 10^{14-16}$ T, where e is the electric charge of the pion, are being generated in noncentral heavy-collisions at the Relativistic Heavy-Ion Collider (RHIC) and the Large-Hadron Collider (LHC) [3, 4]. The presence of strong magnetic fields may be observed in these experiments via the chiral magnetic effect. This effect is basically the separation of charge in a magnetic background due to the existence of topologically nontrivial configurations in the deconfined phase of QCD [5]. Finally, we mention that strong magnetic fields of the order $10^{14} - 10^{19}$ T may have been present in the early universe during the strong and electroweak phase transitions [6, 7]. The presence of a strong

magnetic field at the electroweak phase transition may have implications for baryogenesis, i. e. for the generation of the baryon asymmetry in the universe [8, 9].

Chiral symmetry of the QCD Lagrangian and the spontaneous breaking of this symmetry in the QCD vacuum is an essential feature of the strong interactions. At $T = 0$, it is expected that a constant magnetic background enhances chiral symmetry breaking if it is present already at $B = 0$ or that it induces chiral symmetry breaking if the symmetry is intact at $B = 0$. This phenomenon is called magnetic catalysis and has been discussed in Refs. [10–17] in the context of the Nambu-Jona-Lasinio (NJL) model, chiral perturbation theory, and QED (note however the recent paper [18] where the authors argue that effects from the neutral mesons might show magnetic inhibition if B is strong enough). The basic mechanism is that neutral quark-antiquark pairs minimize their energy by both aligning their magnetic moments along the direction of the magnetic field [1]. Magnetic catalysis was recently demonstrated on the lattice by Braguta et al [19] in three-color quenched QCD as well as by Bali et al [20, 21] in the context of three-color and 1+1+1 flavor QCD. The results of [20, 21], which are for physical quark masses and extrapolated to the continuum limit, are reproduced very well up to magnetic fields of the order $eB \sim 0.1$ (GeV)² in chiral perturbation theory [15, 16] and up to $eB \sim 0.25$ (GeV)² using the Polyakov-loop extended NJL model (PNJL) [22].

Magnetic catalysis at $T = 0$ gives rise to the expectation that the critical temperature T_c for the chiral transition is an increasing function of the magnetic field B . Indeed, ϕ^4 -theory [23], chiral perturbation theory [24, 25] (However, see also Ref. [26]), the NJL model [27, 28],

*Electronic address: arturo.amador@ntnu.no

†Electronic address: andersen@tf.phys.ntnu.no

the PNJL model [22, 29, 30], and the quark-meson (QM) model [28, 31–33] all predict this behavior (note however the recent paper where the authors use a B -dependent scale parameter for the Polyakov loop potential to reproduce the lattice results [34]). Furthermore, the PNJL model also predicts a modest split of approximately 2% between the chiral transition and the deconfinement transition, except for Ref. [35]. In this case the split is of the order 10% and is due to the effects of dimension 8 operators. However, bag-model calculation [36], the Polyakov-loop extended QM calculation [37], and the large- N_c calculation [38] all predict a decreasing critical temperature as a function of B . In Refs. [36, 37], it is probably related to their treatment of vacuum fluctuations and related renormalization issues.

Turning to lattice simulations, the picture seems to be complicated as well. In Refs. [39, 40], the lattice simulations indicate that the chiral critical temperature is increasing as a function of the magnetic field. In this case, the bare quark masses used correspond to a pion mass in the range $M_\pi = 200 - 480$ MeV, i. e. a very heavy pion. These results have been confirmed by Bali et al [20, 21]. However, for light quark masses that correspond to the physical pion mass of $M_\pi = 140$ MeV, their simulations show a critical temperature which is a decreasing function of the magnetic field B . The basic mechanism seems to be that the magnetic catalysis at $T = 0$ turns into inverse magnetic catalysis [41, 42] for temperatures around the critical temperature T_c [43, 44]. The results suggest that the critical temperature is a nontrivial function of the quark masses.

Two-color QCD is interesting for a number of reasons. The order parameter for the deconfinement transition depends on the number of colors N_c . For $N_c = 3$ it is known that the transition is first order and for $N_c = 2$ it is second order. Hence for $N_c = 2$, one expects universality and scaling close to the critical point. For example, the critical exponents will be those of the 2-state Potts model. Moreover, in contrast to three-color QCD, one can perform lattice simulations at finite baryon chemical potential μ_B . The reason is that due to the special properties of the gauge group $SU(2)$, the infamous sign problem is absent and thus importance sampling techniques can be used. Moreover, the physics at finite baryon chemical potential is very different from its three-color counterpart: Again due to the properties of the gauge group, two quarks can form a color singlet and so diquarks are found in the spectrum of the chirally broken phase. The diquarks are bosons and finite baryon chemical potential is then the physics of relativistic bosons and their condensation at low temperature. In the chiral limit, the Lagrangian of two-color two-flavor QCD has an $SU(4)$ symmetry. Since this group is isomorphic to $SO(6)$, chiral symmetry breaking can be cast into the

form $SO(6) \rightarrow SO(5)$. The Goldstone modes are therefore contained in a single five-plet with the usual three pions, a diquark and an antidiquark as well. Various aspects of the phase diagram of two-color QCD can be found e. g. in Refs. [45–57].

The problem of two-color QCD in a strong magnetic background was first investigated on the lattice by Buidovidovich, Chernodub, Lushevskaya, and Polikarpov [58, 59] in the quenched approximation. Magnetic catalysis at $T = 0$ has been verified and in the chiral limit, the chiral condensate grows linearly for small values of B . This behavior is in qualitative agreement with chiral perturbation theory. Later, lattice simulations have been carried out with dynamical fermions by Ilgenfritz, Kalinowski, Müller-Preussker, Petersson, and Schreiber for $N_f = 4$ with identical electric charges [60]. We therefore make no comparison with the result presented here. Their results seem to indicate that the condensate grows linearly with B in the chiral limit at $T = 0$. They also found that for all temperatures and fixed bare quark mass, the chiral condensate grows with the magnetic field. This implies that the critical temperature is an increasing function of the magnetic field.

In the present paper, we use the PNJL model to study two-color QCD in a constant magnetic background B at finite temperature and zero baryon chemical potential. The article is organized as follows. In Sec. II, we briefly discuss the PNJL model in a magnetic field and the thermodynamic potential. In Sec. III, we present our numerical results and in Sec. IV, we summarize and conclude.

II. PNJL MODEL AND THERMODYNAMIC POTENTIAL

In this section, we briefly discuss the two-flavor two-color PNJL model. The Euclidean Lagrangian can be written as

$$\mathcal{L} = \mathcal{L}_0 + \mathcal{L}_1 + \mathcal{L}_2, \quad (1)$$

where the various terms are

$$\mathcal{L}_0 = \bar{\psi}[i\gamma^\mu D_\mu - m_0]\psi, \quad (2)$$

$$\mathcal{L}_1 = G_1 [(\bar{\psi}\psi)^2 + (\bar{\psi}i\gamma_5\psi)^2 + (\bar{\psi}\boldsymbol{\tau}\psi)^2 + (\bar{\psi}i\gamma_5\boldsymbol{\tau}\psi)^2 + |\bar{\psi}^C\sigma_2\tau_2\psi|^2 + |\bar{\psi}^C\gamma_5\sigma_2\tau_2\psi|^2], \quad (3)$$

$$\mathcal{L}_2 = G_2 [(\bar{\psi}\psi)^2 - (\bar{\psi}i\gamma_5\psi)^2 - (\bar{\psi}\boldsymbol{\tau}\psi)^2 + (\bar{\psi}i\gamma_5\boldsymbol{\tau}\psi)^2 - |\bar{\psi}^C\sigma_2\tau_2\psi|^2 + |\bar{\psi}^C\gamma_5\sigma_2\tau_2\psi|^2], \quad (4)$$

where the quark field ψ is an isospin doublet

$$\psi = \begin{pmatrix} u \\ d \end{pmatrix}. \quad (5)$$

The covariant derivative is $D_\mu = \partial_\mu - iqA_\mu - i\sigma_i A_\mu^i$, where A_μ is the gauge field associated with $U(1)$ electromagnetism and A_μ^i is associated with $SU(2)$ color. The covariant derivative is diagonal in flavor space, $q = \text{diag}(2/3, -1/3)|e|$. σ_i ($i = 1, 2, 3$) are the Pauli matrices acting in color space, while τ_i are the Pauli matrices acting in flavor space. m_0 is the mass matrix which is diagonal in flavor space and contains the bare quark masses m_u and m_d . In the following we take $m_u = m_d$. Moreover, ψ^C denotes the charge conjugate of the Dirac spinor, $\psi^C = C\bar{\psi}^T$, where $C = i\gamma^2\gamma^0$. G_1 and G_2 are coupling constants. The interacting part \mathcal{L}_1 is invariant under global $U(4) = SU(4) \times U(1)_A$ transformations while the \mathcal{L}_2 is invariant under global $SU(4)$. One sometimes writes $G_1 = (1 - \alpha)G$ and $G_2 = \alpha G$ and so the parameter α determines the degree of $U(1)_A$ breaking. In the following we choose $\alpha = \frac{1}{2}$.

We next introduce the collective or auxiliary fields

$$\begin{aligned} \sigma &= -2G\bar{\psi}\psi, \pi_i = -2G\bar{\psi}i\gamma_5\tau_i\psi, \rho_i = -2G\bar{\psi}\tau_i\psi, \\ \Delta &= -2G\bar{\psi}i\gamma^5\tau_2\sigma_2\psi^C, \Delta_5 = -2G\bar{\psi}i\tau_2\sigma_2\psi^C, \end{aligned} \quad (6)$$

where σ , π_i , ρ_i , Δ , and Δ_5 have the quantum numbers of a scalar isoscalar, pseudoscalar isovector, scalar isovector, scalar diquark, and pseudoscalar diquark, respectively. The Lagrangian (1) can then be written compactly as

$$\begin{aligned} \mathcal{L} &= \bar{\psi} [i\gamma^\mu D_\mu - m_0 - \sigma - i\gamma^5\tau_i\pi_i - \tau_i\rho_i] \psi \\ &+ \frac{1}{2} \left[\Delta^* \bar{\psi}^C i\gamma^5\tau_2\sigma_2\psi + \text{H. c.} + \Delta_5^* \bar{\psi}^C i\tau_2\sigma_2\psi + \text{H. c.} \right] \\ &- \frac{1}{4G} \left[\sigma^2 + \pi_i^2 + \rho_i^2 + |\Delta|^2 + |\Delta_5|^2 \right]. \end{aligned} \quad (7)$$

If we use the equation of motion for σ , π_i , τ_i , Δ , and Δ_5 to eliminate the auxiliary fields from the Lagrangian (7), we obtain the original Lagrangian (1).

In pure gauge theory, the Polyakov loop Φ , which is the trace of the Wilson line $l(x) = e^{i\int_0^\beta d\tau \sigma_i A_4^i(x, \tau)}$, i. e. $\Phi = \frac{1}{N_c} \text{Tr} e^{i\int_0^\beta d\tau \sigma_i A_4^i(x, \tau)}$, is an order parameter for deconfinement [61]. Under the center symmetry Z_{N_c} , it transforms as $\Phi \rightarrow e^{2\pi n/N_c} \Phi$, where $n = 0, 1, \dots, N_c - 1$. For $N_c = 2$, this is simply a change of sign and in two-color QCD the Polyakov is purely real. At low temperature, i. e. in the confined phase, we have $\Phi \approx 0$ and in the deconfined phase, we have $\Phi \approx 1$. Note, however, that the Polyakov loop is only an approximate order parameter in QCD with dynamical fermions. In the PNJL model, a constant background temporal gauge field A_4 is introduced via the covariant derivative in Eq. (1) [62, 63]. In Polyakov gauge, the background field is diagonal in color space and, $A_4^i = \theta\delta^{i,3}$, where θ is real. The Wilson line can then be written

as $l(x) = \text{diag}(e^{i\beta\theta}, e^{-i\beta\theta})$ and the order parameter Φ reduces to

$$\Phi = \cos(\beta\theta). \quad (8)$$

In order to allow for a chiral condensate, we introduce a nonzero expectation value for the field σ ¹

$$\sigma = -2G\langle\bar{\psi}\psi\rangle + \tilde{\sigma}, \quad (9)$$

where $\tilde{\sigma}$ is a quantum fluctuating fields with vanishing expectation values. To simplify the notation, we introduce the quantity M which is defined by

$$M = m_0 - 2G\langle\bar{\psi}\psi\rangle. \quad (10)$$

Note that the expectation value M is assumed space-time independent in the remainder of this paper. Thus we ignore the possibility of inhomogeneous phases such as the Fulde-Ferrell-Larkin-Ovchinnikov phase as considered in [47]. Eq. (7) is now bilinear in the quark fields and we integrate them out exactly by performing a Gaussian integral. This gives rise to an effective action for the composite fields. In the mean-field approximation, we neglect the fluctuations of the composite fields and the fermionic functional determinant reduces to

$$\begin{aligned} \Omega_{\text{quark}} &= \frac{(M - m_0)^2}{4G} - 4N_c \int \frac{d^3p}{(2\pi)^3} \\ &\times \left\{ E_p + T \log [1 + 2\Phi e^{-\beta E_p} + e^{-2\beta E_p}] \right\}. \end{aligned} \quad (11)$$

where $E_p = \sqrt{p^2 + M^2}$. Note that the integral involving E_p is ultraviolet divergent and requires regularization. We will return to this issue below.

The interpretation of Eq. (11) is now as follows. For $\Phi \approx 0$, we have confinement and thus a thermal part proportional to $T \log[1 + e^{-2\beta E_p}]$, which corresponds to an excitation of energy $2E_p$, i. e. a bound state. Similarly, for $\Phi \approx 1$, the thermal part is $T \log [1 + 2\Phi e^{-\beta E_p} + e^{-2\beta E_p}] = 2T \log[1 + e^{-\beta E_p}]$ which is the thermal contribution from two degrees of freedom each with energy E_p , i. e. the deconfined quark-antiquark pair.

The complete thermodynamic potential Ω is given by the sum of the contributions from the quarks, Ω_{quark} in Eq. (11) and a contribution from the gluons, Ω_{gauge} , where [52]

$$\Omega_{\text{gauge}} = -bT [24\Phi^2 e^{-\beta a} + \log(1 - \Phi^2)] , \quad (12)$$

¹ Since we consider the case of zero quark chemical potential, the other collective fields have zero expectation value.

where a and b are constants. This form is motivated by the lattice strong-coupling expansion [67]. In the pure gauge theory, we can find an explicit expression for the value of the Polyakov loop, $|\Phi| = \sqrt{1 - \frac{1}{24}e^{\beta a}}$ and so $a = T_c \log 24$. Φ goes to zero in a continuous manner showing that the phase transition is second order in agreement with universality arguments [61].

We next consider this system in a constant magnetic field B along the z -axis. We do this by using the covariant derivative $D_\mu = \partial_\mu - iq_a a_\mu - i\sigma_i A_\mu^i$, where $a_\mu = \delta_{\mu,2} x_1 B$ and $A_\mu^i = \delta^{i,3} \delta_{\mu,4} \theta$. Note that the $SU(4)$ symmetry of the Lagrangian is broken in an external magnetic field due to the different electric charges of the u and d quarks. The remaining symmetry is a $U(1)_A$ symmetry which corresponds to a rotation of the u and d quarks by opposite angles [15]. The chiral condensate breaks this Abelian symmetry and it gives rise to a single Goldstone boson, namely the neutral pion.

The energy eigenvalues of the Dirac equations are in this case given by

$$E_m = \sqrt{p_z^2 + M^2 + (2m + 1 - s)|q_f B|}, \quad (13)$$

where M is the mass of the quark, s is the spin of the quark with electric charge q_f and m denotes the m th Landau level. In Eq. (11), dispersion relation E_p is now changed to E_m and the three-dimensional integral becomes a one-dimensional integral and a sum of Landau levels m . For a quark with charge q_f , we then make the replacements

$$\begin{aligned} p^2 &\rightarrow p_z^2 + (2m - 1 + s)|q_f B|, & (14) \\ \int \frac{d^3 p}{(2\pi)^3} &\rightarrow \frac{|q_f B|}{2\pi} \sum_m \int \frac{dp_z}{2\pi}, & (15) \end{aligned}$$

where the sum m is over Landau levels and where the prefactor $\frac{|q_f B|}{2\pi}$ takes into account the degeneracy of the

Landau levels. The divergent term in Eq. (11) is denoted by $\Omega_{\text{quark}}^{\text{div}}$ and now becomes

$$\begin{aligned} \Omega_{\text{quark}}^{\text{div}} &= -N_c \sum_{f,m,s} \frac{|q_f B|}{\pi} \\ &\times \int \frac{dp_z}{2\pi} \sqrt{p_z^2 + M^2 + (2m - 1 + s)|q_f B|}. \end{aligned} \quad (16)$$

The integral over p_z as well as the sum over Landau levels m in Eq. (16) are divergent. We will use zeta-function regularization and dimensional regularization to regulate the divergences. The integral is now generalized to $d = 1 - 2\epsilon$ dimensions using the formula

$$\int \frac{d^d p}{(2\pi)^d} \sqrt{p^2 + M_B^2} = - \left(\frac{e^{\gamma_E} \mu^2}{4\pi} \right)^\epsilon \frac{\Gamma(-\frac{d+1}{2})}{(4\pi)^{\frac{d+1}{2}}} M_B^{d+1}, \quad (17)$$

where $M_B^2 = M^2 + (2m + 1 - s)|q_f B|$ and μ is the renormalization scale in the $\overline{\text{MS}}$ renormalization scheme. This yields

$$\Omega_{\text{quark}}^{\text{div}} = -N_c \left(\frac{e^{\gamma_E} \mu^2}{4\pi} \right)^\epsilon \Gamma(-1 + \epsilon) \sum_{f,m,s} \frac{|q_f B|}{4\pi^2} M_B^{2-2\epsilon}, \quad (18)$$

For each flavor f , the sum over m and s can be written as

$$\sum_{m,s} M_B^{2-2\epsilon} = (2q_f B)^{1-2\epsilon} \left[\zeta(-1 + \epsilon, x_f) - \frac{1}{2} x_f^2 \right], \quad (19)$$

where $\zeta(a, x) = \sum_{n=1}^{\infty} \frac{1}{(a+n)^x}$ is the Hurwitz zeta function and $x_f = \frac{M^2}{2|q_f B|}$. Expanding the Hurwitz zeta function in powers of ϵ , we obtain

$$\Omega_{\text{quark}}^{\text{div}} = \frac{N_c}{16\pi^2} \sum_f \left(\frac{\mu^2}{2|q_f B|} \right)^\epsilon \left[\left(\frac{2(q_f B)^2}{3} + M^4 \right) \left(\frac{1}{\epsilon} + 1 \right) - 8(q_f B)^2 \zeta^{(1,0)}(-1, x_f) - 2|q_f B| M^2 \log x_f + \mathcal{O}(\epsilon) \right], \quad (20)$$

where $\zeta^{(1,0)}(-1, x_f) = \frac{d}{da} \zeta(a, x_f)|_{a=-1}$. The first divergence, which is proportional to $(q_f B)^2$ can be removed by wavefunction renormalization of the tree-level term $\frac{1}{2} B^2$ in the free energy. This term is normally omitted since it is independent of the other parameters of the theory. The second divergent term, which is proportional to M^4 is the identical to the divergence that appears for $B = 0$. We can then add and subtract the term

$$\int \frac{d^d p}{(2\pi)^d} \sqrt{p^2 + M^2} = \left(\frac{\mu}{M} \right)^{2\epsilon} \frac{M^4}{2(4\pi)^2} \left[\frac{1}{\epsilon} + \frac{3}{2} + \mathcal{O}(\epsilon) \right], \quad (21)$$

to Eq. (20) and take the limit $d \rightarrow 3$ in the difference. The divergence is now isolated in the integral on the left-hand-side of Eq. (21). We set $d = 3$ here as well and regulate it by imposing a sharp cutoff Λ in the usual way. Note that the UV cutoff Λ is unrelated to the scale μ in dimensional regularization. The quark thermodynamic potential then becomes

$$\begin{aligned} \Omega_{\text{quark}} = & \frac{(M - m_0)^2}{4G} - \frac{N_c}{4\pi^2} \left[\Lambda \sqrt{\Lambda^2 + M^2} (2\Lambda^2 + M^2) + M^4 \log \frac{\Lambda + \sqrt{\Lambda^2 + M^2}}{M} \right] \\ & - \frac{N_c}{16\pi^2} \sum_f (q_f B)^2 [8\zeta'(-1, x_f) - 4(x_f^2 - x_f) \log x_f + 2x_f^2] \\ & - \sum_{f,m,s} \frac{|q_f B| T}{2\pi} \int_0^\infty \frac{dp_z}{2\pi} \log \left[1 + 2\Phi e^{-\beta E_m} + e^{-2\beta E_m} \right]. \end{aligned} \quad (22)$$

The complete thermodynamic potential in a constant magnetic background is the sum of Eqs. (12) and (22) and denoted by Ω . The values of M and the Polyakov loop Φ are found by minimizing Ω with respect to M and Φ , i. e. by solving the gap equations

$$\frac{\partial \Omega}{\partial M} = 0, \quad \frac{\partial \Omega}{\partial \Phi} = 0. \quad (23)$$

Using Eqs. (22), we obtain

$$\begin{aligned} & \frac{(M - m_0)}{2G} - \frac{N_c}{2\pi^2} \left[\Lambda \sqrt{\Lambda^2 + M^2} + \frac{\Lambda^2(2\Lambda^2 + M^2)}{\sqrt{\Lambda^2 + M^2}} + 2M^2 \log \frac{\Lambda + \sqrt{\Lambda^2 + M^2}}{M} \right] \\ & + \frac{M^4}{\Lambda^2 + M^2 + \Lambda \sqrt{\Lambda^2 + M^2}} - M^3 \Big] - \frac{N_c}{16\pi^2} \sum_f M |q_f B| \left[8\zeta'(0, x_f) - 4(2x_f - 1) \log x_f + 8x_f \right] \end{aligned} \quad (24)$$

$$\begin{aligned} & + \frac{N_c}{2\pi^2} \sum_{f,m,s} |q_f B| \int_0^\infty dp_z \frac{M}{E_m} \frac{\Phi e^{-\beta E_m} + e^{-2\beta E_m}}{1 + 2\Phi e^{-\beta E_m} + e^{-2\beta E_m}} = 0, \\ & b\Phi \left[\frac{1}{1 - \Phi^2} - 24e^{-\beta a} \right] - \sum_{f,m,s} \frac{|q_f B|}{2\pi} \int \frac{dp_z}{2\pi} \frac{E^{-\beta E_m}}{1 + 2\Phi e^{-\beta E_m} + e^{-2\beta E_m}} = 0. \end{aligned} \quad (25)$$

We notice in particular that $\Phi = 0$ is the only solution to Eq. (25) at $T = 0$ and the PNJL model then reduces to the NJL model.

III. NUMERICAL RESULTS

The PNJL model has five different parameters, namely G , m_0 , and Λ in Ω_{quark} and a and b in Ω_{gauge} . At $T = 0$, $\Omega_{\text{gauge}} = 0$ and so the PNJL model reduces to the NJL model. We can therefore determine the parameters G , m_0 , and Λ separately. For $N_c = 3$, one normally chooses an ultraviolet cutoff Λ and tunes the parameters m_0 and G such that one reproduces the pion mass M_π and the pion decay constant F_π in the vacuum. For $N_c = 2$, we have no experiments to guide us and several

different choices have been made [48, 52, 64]. We follow Ref. [52] that uses N_c scaling arguments. Since the pion decay constant is proportional to $\sqrt{N_c}$ and the pion mass is proportional to N_c , we simply rescale the three-color values by $\sqrt{\frac{2}{3}}$ and $\frac{2}{3}$, respectively. This scaling gives $f_\pi = 75.4$ MeV and $m_\pi = 93.3$ MeV. Note that we in the following refer to the case where $m_\pi = 93.3$ MeV as the physical point. In order to facilitate the comparison with similar plots in the literature where $N_c = 3$, $|qB|$ is given in units of $M_\pi^2 = (140\text{MeV})^2$ and the scaling of the thermodynamic potential is done by dividing by F_π^4 , where $F_\pi = 93$ MeV, i. e. the $N_c = 3$ values of the pion mass and the pion decay constant. With an ultraviolet cutoff of $\Lambda = 657$ MeV, this gives $G = 7.23$ (GeV)⁻² and $m_0 = 5.4$ MeV at the physical point and $G = 7.00$ (GeV)⁻² and $m_0 = 0$ MeV in the chiral limit.

The parameter a in Ω_{gauge} is related to the critical temperature for deconfinement transition in pure-gluon QCD and reads $a = T_c \log 24$. In the pure gauge theory, T_c is independent of the number of colors N_c [65] to a first approximation, see however Ref. [66] for a recent study for $4 \leq N_c \leq 8$. We will therefore use the critical temperature for pure-gluon QCD from lattice calculations with $N_c = 3$, $T_c = 270$ MeV. This yields $a = 858.1$ MeV. The parameter b can be tuned so that the chiral transition takes place at approximately the same temperature as the deconfinement transition. Note, however, that the Polyakov loop is strictly not an order parameter in the presence of dynamical fermions. It is a crossover and the transition region is defined as a band in which Φ varies. We define the transition region to be the temperatures where $0.4 < \Phi < 0.6$ and the width of the band in the B - T plane tells one how fast the crossover is. Nevertheless, we define a deconfinement temperature by the condition $\Phi = \frac{1}{2}$. This gives a curve in the B - T plane and acts a useful guide to the eye. The requirement $\Phi = \frac{1}{2}$ yields $b = (210.5)^3$ (MeV)³. We finally point out that instead of using the criteria for the deconfinement and chiral transition mentioned above, it is common to define T_c by the inflection point of the appropriate order parameter as a function of T . We have performed a few sample calculations to compare the two criteria. For both transitions the difference between them is less than one percent.

In Fig. 1, we show the normalized constituent quark mass M/M_0 (solid line), where M_0 is the quark mass at $T = 0$, and the Polyakov loop (dashed line) in the chiral limit as a function of T/M_π , where $M_\pi = 140$ MeV is the pion mass in the vacuum for $N_c = 3$. The quark mass vanishes at the temperature at which $\Phi = \frac{1}{2}$. Thus for $|qB| = 0$, the two transitions take place at the same temperature as explained above². For comparison, we also plot the chiral condensate in the NJL model (dotted line) as well as the Polyakov loop in the pure-gluon case (dash-dotted line), i.e. as derived from the potential Ω_{gauge} in Eq. (12). The chiral transition in the chiral limit is second order for $|qB| = 0$ in the NJL as well as in the PNJL model.

In Fig. 2, we show the chiral condensate $\langle \bar{\psi}\psi \rangle_B$ normalized to the chiral condensate in the vacuum $\langle \bar{\psi}\psi \rangle_0$ as a function of $|qB|$ in the chiral limit and at the physical point in the vacuum i.e. $T = \mu_B = 0$ in the PNJL model. Note that here and in the following $|qB|$ is measured in units of the pion mass for $N_c = 3$, i. e. $M_\pi = 140$ MeV. Since the effects of the Polyakov van-

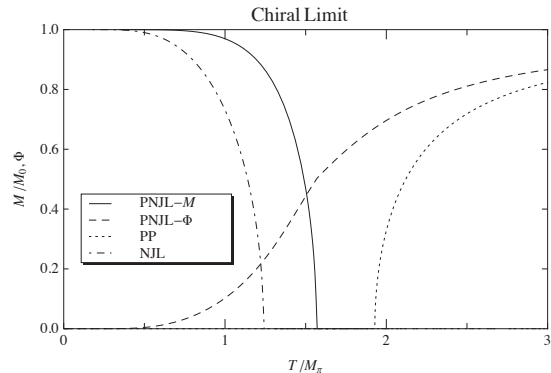


FIG. 1: Normalized constituent quark mass and Polyakov loop in the chiral limit as a function of T/M_π , where $M_\pi = 140$ MeV is the pion mass for $N_c = 3$. See main text for details.

ish in the vacuum this is also the prediction of the NJL model. $\langle \bar{\psi}\psi \rangle_B$ is a monotonically increasing function of $|qB|$ and the system exhibits magnetic catalysis. In the NJL model and in the PNJL model at zero temperature, it is known that the chiral condensate grows quadratically with the field for small $|qB|$ in the chiral limit [10, 14]. This is in contrast to chiral perturbation theory where the dependence is linear. In Ref. [58] the authors investigate the chiral condensate as a function of the magnetic field B for $SU(2)$ gauge theory using lattice simulations in the quenched approximation. The authors found that the linear behavior found in chiral perturbation theory can be described qualitatively by the function $\Sigma(B) = \Sigma_0 \left(1 + \frac{|qB|}{\Lambda_B^2}\right)$, where Σ_0 and Λ_B are fitting parameters. The parameters depend on the lattice parameters and we are using the value $\Lambda_B = 1.53$ GeV, which corresponds to their largest lattice and their smallest lattice spacing a . The result is shown as the long-dashed line in Fig. 2 and is seen to agree reasonably well for magnetic field up to $|qB| \approx 6M_\pi^2$

We next consider the magnetic moment for a fermion of flavor f . In terms of the spin operator $\Sigma^{\mu\nu} = \frac{1}{2i}(\gamma^\mu\gamma^\nu - \gamma^\nu\gamma^\mu)$, it is defined by $\langle \bar{\psi}_f \Sigma^{\mu\nu} \psi_f \rangle$. In the case of constant magnetic field in the z -direction, only $\Sigma_f \equiv \Sigma^{12}$ is nonzero [68]. Using the properties of the γ -matrices, it can be shown that only the lowest Landau level (LLL) contributes to the expectation value of Σ_f and reads

$$\langle \bar{\psi}_f \Sigma_f \psi_f \rangle_B = \langle \bar{\psi}_f \psi_f \rangle_B^{\text{LLL}}, \quad (26)$$

where the superscript indicates that we include only the

² In the chiral limit the normalized chiral condensate and the normalized constituent quark mass are the same, cf. Eq. (10).

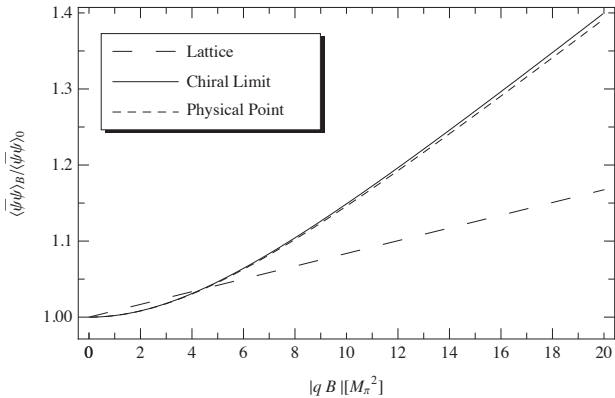


FIG. 2: The chiral condensate $\langle \bar{\psi}\psi \rangle_B$ normalized to the chiral condensate in the vacuum $\langle \bar{\psi}\psi \rangle_0$ as a function of magnetic field $|qB|$ in the chiral limit (solid line) and at the physical point (dashed line) at zero temperature. Here $M_\pi = 140$ MeV is the pion mass for $N_c = 3$. Lattice results for pure-gluon $SU(2)$ from Ref. [58] is shown for comparison (long-dashed line).

lowest Landau level. We then define the polarization by

$$\begin{aligned} \mu_f &= \frac{\langle \bar{\psi}_f \Sigma_f \psi_f \rangle_B}{\langle \bar{\psi}_f \psi_f \rangle_B} \\ &= 1 - \frac{\langle \bar{\psi}_f \psi_f \rangle_B^{\text{HLL}}}{\langle \bar{\psi}_f \psi_f \rangle_B}, \end{aligned} \quad (27)$$

where the superscript HLL indicates that we have included only the higher Landau levels. In Fig. 3, we show the polarization $\mu = \frac{1}{2}(\mu_u + \mu_d)$ at $T = 0$ and in the chiral limit as a function of $|qB|$. As expected, the polarization saturates for large magnetic fields to $\mu^\infty = 1$. In this limit, the fermions in the higher Landau levels effectively become very heavy (cf. Eq. (13)), they decouple and the LLL dominates the physics. In this limit all the fermions are in the LLL and their spin is pointing in the same direction. The ratio of the mass of the fermions in the LLL and those in the HLL is essentially given by the dimensionless ratio $M^2/|qB|$. This ratio changes where the curve is steep and levels off for large values of $|qB|$.

In Fig. 4, we show the critical temperature for the chiral transition (solid line) and the critical temperature for the deconfinement transition (dashed line) as functions of the magnetic field in the chiral limit for the PNJL model. The band is defined by $0.4 < \Phi < 0.6$ and shows the transition region for the deconfinement transition. We also show the critical temperature in the NJL model for comparison. The parameter b in Eq. (12) has

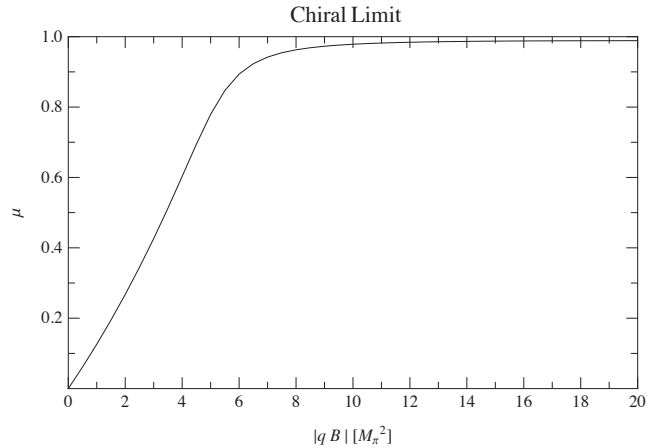


FIG. 3: The polarization μ as a function of $|qB|$ in the chiral limit and at zero temperature. Here $M_\pi = 140$ MeV is the pion mass for $N_c = 3$.

been tuned such that the two transitions coincide for $B = 0$. We note that there is a splitting between the two transitions and that T_c for the deconfinement is always lower than T_c for the chiral transition and that the gap increases as a function of B . Thus, there should be a phase in which matter is deconfined and chiral symmetry is broken. The splitting was also observed in Ref. [22, 29, 35, 37, 42, 69], where the authors coupled the Polyakov loop to linear sigma model with quarks with $N_c = 3$ colors. We first note that T_c is decreasing ever so slightly from $|qB| = 0$ to $|qB| \approx M_\pi^2$ and then increasing again. This is in contrast to the NJL model where T_c is monotonically increasing as a function of $|qB|$. We discuss this further below.

Moreover, while T_c for the chiral transition increases by more than 20% from $B = 0$ to $|qB| = 20M_\pi^2$, T_d for the deconfinement transition is hardly affected. The width of the band is approximately 30 MeV. In contrast, the lattice simulations for $N_c = 2$ reported in Ref. [60] indicate that the critical temperature for deconfinement coincide with that of the chiral transition. Finally, we note that the determination of a and b has changed the critical temperature for the chiral transition dramatically. The increase of T_c at $B = 0$ is approximately 35 MeV and is fairly constant up to $|qB| = 20$ MeV. In order to compare the chiral transition at finite magnetic field in the NJL and PNJL model, i. e. the effects of the Polyakov loop, there might be other ways of determining a and b . For example, one could force the deconfinement transition and the chiral transition in the PNJL model to take place at the same temperature for $B = 0$ and force it to coincide with the chiral transition in the NJL

model as well. This way of determining the parameters in Ω_{gauge} would not require the input from lattice simulations.

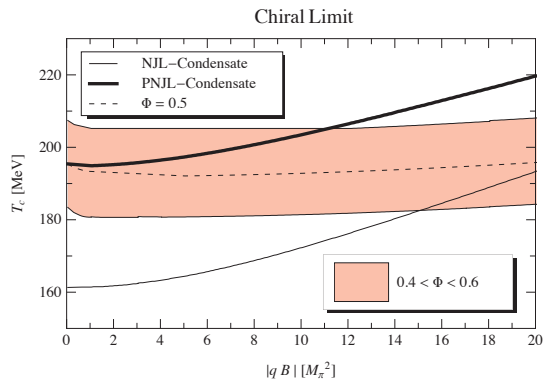


FIG. 4: Critical temperature for the chiral transition (solid line) and critical temperature for the deconfinement transition (dashed line) as functions of magnetic field $|qB|$ in the chiral limit for the PNJL model. The band is defined by $0.4 < \Phi < 0.6$. We also show the critical temperature for the chiral transition (thin line) in the NJL model. Here $M_\pi = 140$ MeV is the pion mass for $N_c = 3$.

In Fig. 5, we show the thermodynamic potential $\Omega - \Omega_0$ divided by F_π^4 in the chiral limit for four different temperatures and $|qB| = 20M_\pi^2$. For each temperature, we also give the value of the Polyakov loop. The critical temperature for the chiral transition is $T_c = 220$ MeV and from the long-dashed line we see that transition is second order. Since the value of the Polyakov loop for $T = 220$ MeV is $\Phi = 0.68$, we conclude that the deconfinement transition has already taken place.

In Fig. 6, we show the thermodynamic potential $\Omega - \Omega_0$ divided by F_π^4 as a function of Φ in the chiral limit for four different temperatures and $|qB| = 20M_\pi^2$. For each temperature, we also give the value of the chiral condensate M . At $T = 197$ MeV, we find that the minimum of the effective potential occurs for $\Phi = \frac{1}{2}$ which defines the critical temperature for the deconfinement transition in the chiral limit. At this temperature, $M = 286.2$ MeV and so we are still in the chirally broken phase. For $T = 250$ MeV, the chiral condensate is vanishing and so we are in the chirally symmetric deconfined phase. In the chiral limit, the chiral transition is always second order.

At the physical point, the chiral transition is a crossover and there is no well-defined critical temperature T_c at which the chiral condensate vanishes. However, one can define a pseudo-critical temperature by the inflection point of the chiral condensate as a func-

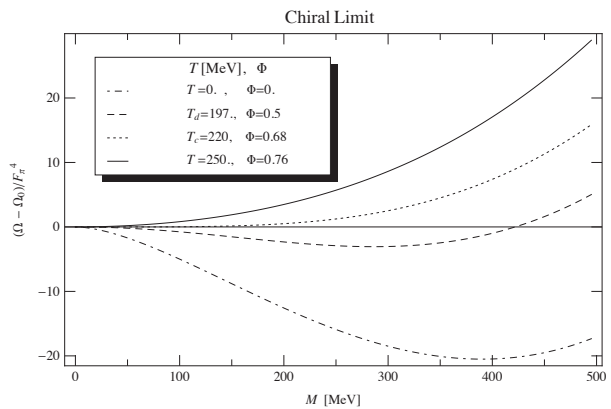


FIG. 5: Thermodynamic potential $\Omega - \Omega_0$ divided by F_π^4 as a function of M in the chiral limit for four different temperatures and $|qB| = 20M_\pi^2$. Here $M_\pi = 140$ MeV and $F_\pi = 93$ MeV are the values for the pion mass and the pion decay constant for $N_c = 3$. See main text for details.

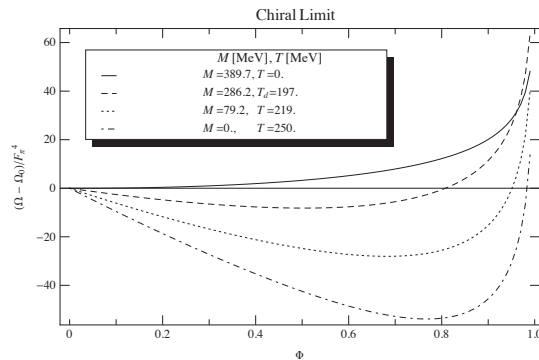


FIG. 6: Thermodynamic potential $\Omega - \Omega_0$ divided by F_π^4 as a function of Φ in the chiral limit for four different temperatures and $|qB| = 20M_\pi^2$. Here $M_\pi = 140$ MeV and $F_\pi = 93$ MeV are the values for the pion mass and the pion decay constant for $N_c = 3$. See main text for details.

tion of temperature. One can also define the transition region by the temperature range where M varies between 0.4 and 0.6. This range depends on the magnetic field and gives rise to a band in the B - T plane. This is shown as the dark band in Fig. 7. In the same manner, we define the crossover transition for the deconfinement transition by the the temperature range where $0.4 < \Phi < 0.6$. This is shown as the light band in Fig. 7. Moreover, as a guide to the eye, we also show the lines where $M/M_0 = \frac{1}{2}$ and $\Phi = \frac{1}{2}$, respectively. For comparison, we also show the pseudocritical temperature for the chiral transition in the NJL model (dashed

line). The curves indicate that the two transitions coincide for magnetic fields up to $|qB| \approx 5M_\pi^2$ and after that they split. The deconfinement transition is always taking place first. We notice that T_c for the chiral transition first decreases as a function of $|qB|$ until $|qB| \approx 3M_\pi^2$ and then it starts to increase again. At the physical point where there is only a cross-over, the width of the transition is much bigger than this decrease in T_c . The difference between $T_c(|qB| = 0)$ and $T_c(|qB| = 3M_\pi^2)$ is only a few MeV which is comparable to the drop found by Bali et al. [20, 21] for $N_c = 3$. However, note that these authors find that T_c is decreasing as a function in the entire region they investigated, namely magnetic fields up to $|qB| \approx 1 \text{ (GeV)}^2$, and that the drop in T_c is approximately 20 MeV in this range. The non-monotonic behavior of T_c as a function of $|qB|$ in the PNJL model is absent in the NJL model and we attribute this to the coupling to the Polyakov loop. Another possible explanation for the non-monotonic behaviour is that it could be very well an artifact of our mean field approximation. Finally, we note that the band of the chiral transition is much narrower than that of the deconfinement transition (approximately $T = 10 \text{ MeV}$ versus approximately $T = 30 \text{ MeV}$) and is so significantly faster. In

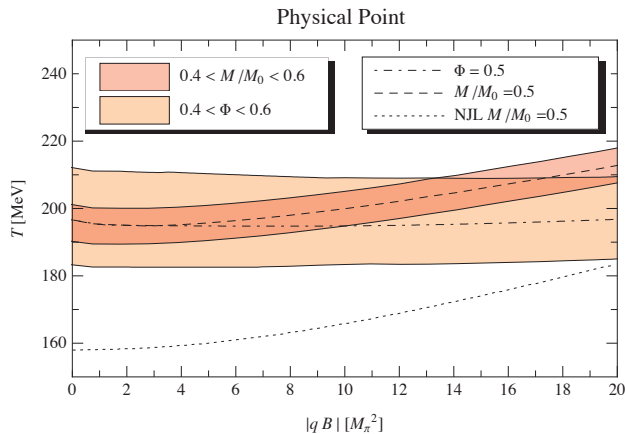


FIG. 7: Transition region at the physical point as a function of $|qB|$. Here $M_\pi = 140 \text{ MeV}$ is the value for the pion mass for $N_c = 3$. For comparison, the dashed line shows the pseudocritical temperature in the NJL model. See main text for details.

IV. CONCLUDING REMARKS

In the present paper, we have considered two-color two-flavor QCD in a constant magnetic background us-

ing the PNJL model. In the chiral limit, the chiral transition is always second order with mean-field critical exponents. The order of the transition is in agreement

Chiral Limit

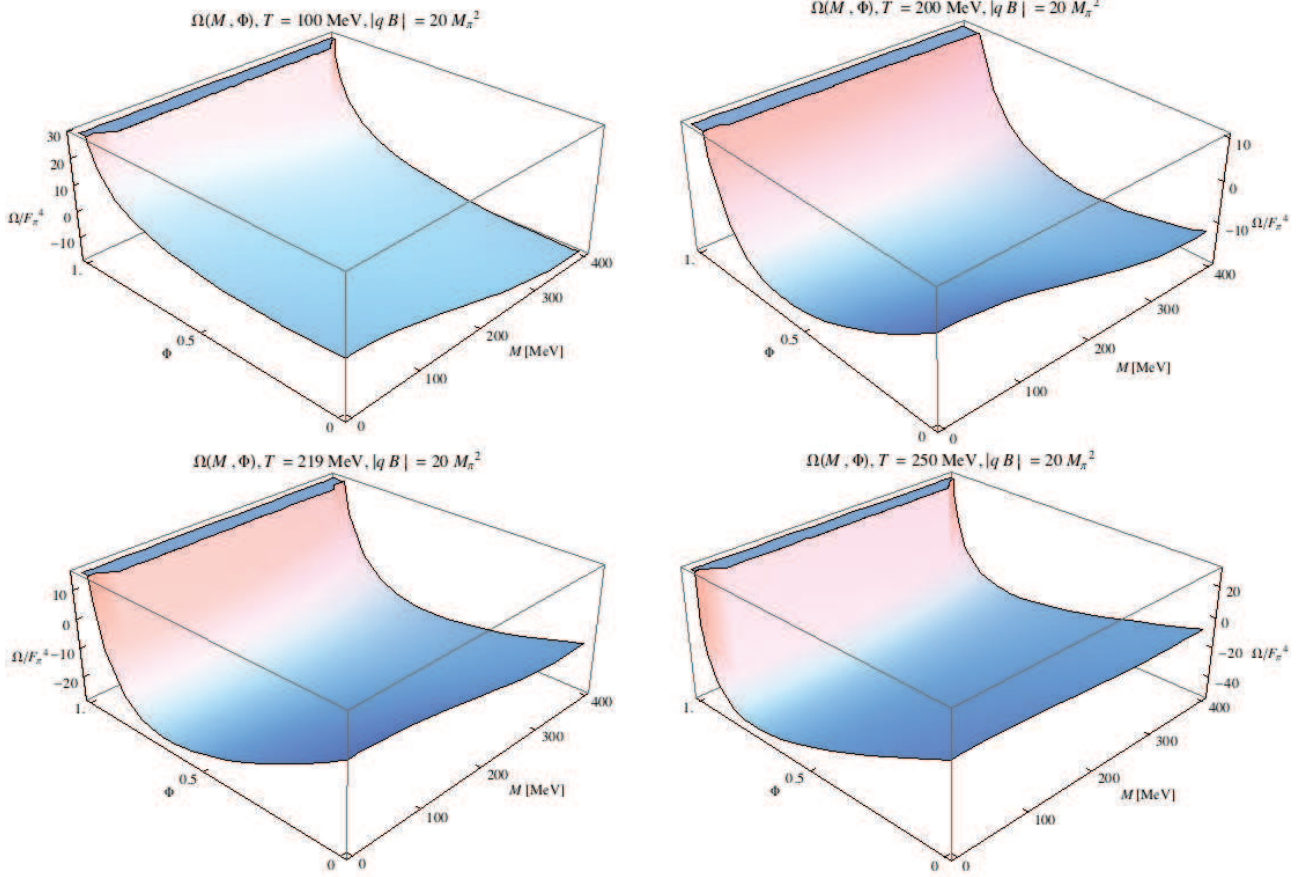


FIG. 8: The normalized thermodynamic potential $(\Omega - \Omega_0)/F_\pi^4$ in the chiral limit as a function of M and Φ for four different temperatures and $|qB| = 20M_\pi$. From left to right $T = 100$ MeV, $T = 200$ MeV, $T = 219$ MeV, and $T = 250$ MeV. Here $M_\pi = 140$ MeV and $F_\pi = 93$ MeV are the values for the pion mass and the pion decay constant for $N_c = 3$. See main text for details.

with universality arguments. Our results for the chiral transition as a function of $|qB|$ shows some interesting behavior: the critical temperature first decreases and then it increases. This behavior is more pronounced at the physical point (cf. Figs. 4 and 7). In this case the transition temperature decreases for values of $|qB|$ up to approximately $3M_\pi^2$ and then it increases. We therefore have inverse magnetic catalysis in this range of $|qB|$ and results from the coupling to the Polyakov loop since the transition temperature is increasing for all values of $|qB|$ in the NJL model. Even though we attribute the coupling to the Polyakov loop as the mechanism responsible for the inverse catalysis in the range mentioned, there

is the possibility that this effect is actually an artifact of the mean-field approximation we use in our calculations and it would not survive if we used more advanced techniques. For example it is known that critical points in the $\mu - T$ plane in some low-energy effective theories display a critical endpoint in mean-field calculations. If one uses functional renormalization techniques, they disappear [55]. Thus, it is worthwhile pursuing this behaviour using more sophisticated methods before we conclude more firmly about the nature of this effect. The lattice simulations of Ref. [60] seem to indicate a transition temperature which is increasing with the strength of the magnetic field. However, one must be cautious since

they did not take the continuum limit and used $N_f = 4$ with identical electric charges. A careful study using 1+1 flavors, $N_c = 2$, and taking the continuum limit is necessary to compare with the results in the present paper.

We next turn to the case $N_c = 3$. The inverse catalysis for temperature around T_c seen in [20, 21, 43, 44] hinges on taking continuum limit and using physical quark masses. For larger unphysical quark masses, the system shows catalysis at finite temperatures. Given the lattice results for $N_c = 3$ it is clear that all the model cal-

culations to date fail at temperatures T around T_c and in particular does not incorporate that magnetic catalysis is turned into inverse magnetic catalysis around the transition. This is independent of whether it is a mean-field calculation or one goes beyond using e.g. functional renormalization group techniques [31, 32]. In the recent papers [43, 44], the authors provide a plausible explanation for the discrepancy between the model calculations and the lattice simulations. The chiral condensate can be written as

$$\langle \bar{\psi}\psi \rangle = \frac{1}{\mathcal{Z}(B)} \int d\mathcal{U} e^{-S_g} \det(\mathcal{D}(B) + m) \text{Tr}(\mathcal{D}(B) + m)^{-1}, \quad (28)$$

where the partition function is

$$\mathcal{Z}(B) = \int d\mathcal{U} e^{-S_g} \det(\mathcal{D}(B) + m), \quad (29)$$

and S_g is the pure-gluon action. Thus there are two contributions to the chiral condensate, namely the operator itself (coined valence contribution) and the change of typical gauge configurations sampled, coming from the determinant in Eq. (28) (coined sea contribution). At least for small magnetic fields one can disentangle these contributions by defining

$$\langle \bar{\psi}\psi \rangle^{\text{val}} = \frac{1}{\mathcal{Z}(0)} \int d\mathcal{U} e^{-S_g} \det(\mathcal{D}(0) + m) \text{Tr}(\mathcal{D}(B) + m)^{-1}, \quad (30)$$

$$\langle \bar{\psi}\psi \rangle^{\text{sea}} = \frac{1}{\mathcal{Z}(B)} \int d\mathcal{U} e^{-S_g} \det(\mathcal{D}(B) + m) \text{Tr}(\mathcal{D}(0) + m)^{-1}. \quad (31)$$

At zero temperature, both contributions are positive leading to magnetic catalysis. At temperatures around the transition temperature, the valence condensate is still positive while the sea condensate is negative. Hence there is a competition between the two leading to a net inverse catalysis. The sea contribution can be viewed as a back reaction of the fermions on the gauge fields and this effect is not present in the model calculations as there are no dynamical gauge fields. If such a back reaction can be mimicked or incorporated in the model calculations, one may be able to obtain agreement with the lattice simulations.

It is also interesting to note that the magnetic field hardly affects the critical temperature for deconfinement. This is in line with the observation of [30]. Moreover, our results seem to indicate that the two transitions coincide at the physical point up to fairly large values of the magnetic field. $|qB| \approx 5M_\pi^2$.

Finally, we would like to comment on the role of quantum fluctuations and related renormalization issues. In a

one-loop calculation of the effective potential it is possible to separate the vacuum contributions from the thermal contributions. In some cases, it therefore makes sense to investigate the role of the vacuum fluctuations. For example, in the QM, it is customary to treat the bosons at tree level and the fermions at the one-loop level. In this case it was shown in Ref. [70] for $B = 0$ that the order of the phase transition depends whether the zero-temperature fluctuations are included or not; if they are, the chiral transition is second order and if they are not, it is first order. The same effect of the vacuum fluctuations were found in the entire μ_B - T plane in strong magnetic fields in [33]. In contrast to the QM model with quarks, this question does not make sense in the (P)NJL model. The reason is that chiral symmetry breaking in the (P)NJL is always a loop effect in contrast to the QM model where it is built into the tree-level potential. In a similar manner, Ref. [71] finds that a crossover transition (for $N_c = 3$) at the physical point remains a crossover at finite magnetic field B in an NJL model

calculation. This is in contrast to Ref. [30] where it is found that strong magnetic fields turn the crossover into a first-order transition. In their work, the authors use the QM model and renormalize by subtracting the fermionic vacuum fluctuations at $B = 0$.

Acknowledgments

J. O. A. would like to thank Tomas Brauner for useful discussions.

-
- [1] Lect. Notes Phys. "Strongly interacting matter in magnetic fields" (Springer), edited by D. Kharzeev, K. Landsteiner, A. Schmitt, and H.-U. Yee.
- [2] R. C. Duncan and C. Thompson, *Astrophys. J.* **392** L9 (1992).
- [3] V. Skokov, A. Y. Illarionov, and V. Toneev, *Int. J. Mod.Phys. A* **24** 5025, (2009).
- [4] A. Bzdak and V. Skokov, *Phys.Lett. B* **710**, 171 (2012).
- [5] D. E. Kharzeev, L. D. McLerran, and H. J. Warringa, *Nucl. Phys. A* **803**, 227 (2008).
- [6] T. Vachaspati, *Phys. Lett. B* **265**, 258 (1991).
- [7] K. Enqvist and P. Olesen, *Phys. Lett. B* **319**, 178 (1993).
- [8] M. Laine, K. Kajantie, M. Laine, J. Peisa, K. Rummukainen, M. E. Shaposhnikov, *Nucl. Phys. B* **544**, 357 (1999).
- [9] A. De Simone, G. Nardini, M. Quiros, and A. Riotto, *JCAP* 1110, 030 (2011).
- [10] S. P. Klevansky and R. H. Lemmer, *Phys. Rev. D* **39**, 3478, (1989).
- [11] K.G. Klimenko, *Z. Phys. C* **54**, 323 (1992).
- [12] V. P. Gusynin, V. A. Miransky, and I. A. Shovkovy, *Phys. Rev. Lett.* **73**, 3499 (1994).
- [13] V. P. Gusynin, V.A. Miransky, and I. A. Shovkovy, *Nucl. Phys. B* **462**, 249 (1996).
- [14] D. Ebert, K. G. Klimenko, M. A. Vdovichenko, and A. S. Vshivtsev, *Phys. Rev. D* **61** 025005 (1999).
- [15] I. Shushpanov and A. V. Smilga, *Phys. Lett. B* **402** 351, (1997).
- [16] T. D. Cohen, D. A. McGady, and E. S. Werbos, *Phys. Rev. C* **76**, 055201 (2007).
- [17] K. Fukushima and J. M. Pawłowski, *Phys. Rev. D* **86**, 076013 (2012).
- [18] K. Fukushima and Y. Hidaka, *Phys. Rev. Lett.*, **110**, 031601 (2013).
- [19] V. V. Braguta, P. V. Buividovich, T. Kalaydzhyan, S. V. Kuznetsov, and M. I. Polikarpov, PoS LATTICE2010, 190 (2010), *Phys. Atom. Nucl.* **75**, 488 (2012).
- [20] G. S. Bali, F. Bruckmann, G. Endrödi, Z. Fodor, S. D. Katz, S. Krieg, A. Schafer, and K. K. Szabo, *JHEP* **1202**, 044 (2012).
- [21] G. S. Bali, F. Bruckmann, G. Endrödi, Z. Fodor, S.D. Katz, and A. Schafer, *Phys. Rev. D* **86**, 071502 (2012)
- [22] R. Gatto and M. Ruggieri, *Phys. Rev. D* **82**, 054027 (2010).
- [23] D. C. Duarte, R. L. S. Farias, and R. O. Ramos, *Phys. Rev. D* **84**, 083525 (2011).
- [24] N. O. Agasian, *Phys. Lett. B* **488**, 39 (2000).
- [25] J. O. Andersen, *Phys. Rev. D* **86**, 025020 (2012); *JHEP* **1210**, 005 (2012).
- [26] N. O. Agasian and S. M. Fedorov, *Phys. Lett. B* **663**, 445 (2008).
- [27] S. S. Avancini, D. P. Menezes, M. B. Pinto, and C. Providencia, *Phys.Rev. D* **85** 091901 (2012).
- [28] G. N. Ferrari, A. F. Garcia, and M. B. Pinto, *Phys. Rev. D* **86**, 096005 (2012).
- [29] K. Fukushima, M. Ruggieri, and R. Gatto, *Phys. Rev. D* **81**, 114031 (2010).
- [30] E. S. Fraga and A. J. Mizher, *Phys. Rev. D.* **78**, 025016 (2008).
- [31] V. Skokov, *Phys. Rev. D* **85**, 03426 (2012).
- [32] J. O. Andersen and A. Tranberg, *JHEP* **1208**, 002 (2012).
- [33] J. O. Andersen and R. Khan, *Phys. Rev. D* **85**, 065026 (2012).
- [34] M. Ferreira, P. Costa, D. P. Menezes, C. Providencia, N. Scoccola, arXiv:1305.4751v1 [hep-ph].
- [35] R. Gatto and M. Ruggieri, *Phys. Rev. D* **83**, 034016 (2011).
- [36] E. S. Fraga and L. F. Palhares, *Phys. Rev. D* **86**, 016008 (2012).
- [37] A. J. Mizher, M. N. Chernodub and E. S. Fraga, *Phys. Rev. D* **82**, 105016 (2010).
- [38] E. S. Fraga, J. Noronha, and L. F. Palhares, *Phys. Rev. D* **87**, 114014 (2013).
- [39] M. D'Elia, S. Mukherjee, and F. Sanfilippo, *Phys. Rev. D* **82**, 051501 R (2010).
- [40] M. D'Elia and F. Negro, *Phys. Rev. D* **83**, 114028 (2011).
- [41] T. Inagaki, D. Kimura, and T. Murata, *Prog. Theor. Phys.* **111**, 371 (2004).
- [42] F. Preis, Anton Rebhan, and Andreas Schmitt. *JHEP* **1103**, 033 (2011).
- [43] G. S. Bali, F. Bruckmann, G. Endrodi, F. Gruber, and A. Schaefer *JHEP* **1304** 130 (2013).
- [44] F. Bruckmann, G. Endrodi, and T. G. Kovacs, *JHEP* **1304**, 112 (2013).
- [45] L. A. Kondratyuk and M. M. Gianinni, *Phys. Lett. B* **269** 139 (1991).
- [46] J. B. Kogut, M. A. Stephanov, and D. Toublan, *Phys. Lett. B* **464**, 183 (1999).
- [47] K. Splittorff, D.T. Son, and M. A. Stephanov, *Phys. Rev. D* **64**, 016003 (2001).
- [48] C. Ratti and W. Weise, *Phys. Rev. D* **70**, 054013 (2004).
- [49] P. Cea, L. Cosmai, M. D'Elia, and A. Papa *JHEP* **0702**, 066 (2007.)
- [50] S. Hands, S. Kim, J-I. Skullerud, *Phys. Rev. D* **81** 091502 (2010).
- [51] T. Kanazawa, Tilo Wettig, N. Yamamoto, *JHEP* **0908**,

- 003 (2009).
- [52] T. Brauner, K. Fukushima, and Y. Hidaka Phys. Rev. D **80**, 074035 (2009); Erratum-ibid. D **81**, 119904 (2010).
- [53] J. O. Andersen and T. Brauner, Phys. Rev. D **81**, 096004 (2010).
- [54] T. Zhang, T. Brauner, A. Kurkela, A. Vuorinen, JHEP **1202**, 139 (2012).
- [55] N. Strodthoff, B.-J. Schaefer, L. von Smekal, Phys. Rev. D **85**, 074007 (2012).
- [56] K. Kashiwa, T. Sasaki, and H. Kounu, Phys. Rev. D **87** 016015 (2013).
- [57] S. Imai, H. Toki, and W. Weise e-Print: arXiv:1210.1307 [nucl-th].
- [58] P. V. Buividovich, M. N. Chernodub, E. V. Luschevskaya, and M. I. Polikarpov, Phys. Lett. B **682**, 484 (2010).
- [59] P. V. Buividovich, M. N. Chernodub, E. V. Luschevskaya, and M. I. Polikarpov, Nucl. Phys. B **826**, 313 (2010).
- [60] E.-M. Ilgenfritz, M. Kalinowski, M. Müller-Preussker, B. Petersson, and A. Schreiber, Phys. Rev. D **85**, 114504 (2012).
- [61] B. Svetitsky and L. G. Yaffe, Nucl. Phys. B **210**, 423 (1982).
- [62] K. Fukushima, Phys. Lett. B **591**, 277 (2004).
- [63] E. Megias, E. Ruiz Arriola, and L.L. Salcedo, Phys. Rev. D **74**, (2006) 065005; ibid **74**, 114014 (2006).
- [64] G.-F. Sun, L. He, P. Zhuang, Phys. Rev. D **75**, 096004 (2007).
- [65] C. Sasaki, B. Friman, and K. Redlich, Phys. Rev. D **75**, 074013 (2007).
- [66] B. Lucini, A. Rago, and E. Rinaldi, Phys. Lett. B **712** 279 (2012).
- [67] K. Fukushima, Phys. Rev. D **77**, 114028 (2008).
- [68] M. Frasca and M. Ruggieri, Phys. Rev. D **83**, 094024 (2011).
- [69] N. Callebaut, D. Dudal, and H. Verschelde, PoS FACESQCD 046 (2010).
- [70] V. Skokov, B. Friman, E. Nakano, K. Redlich, and B.-J. Schaefer, Phys.Rev. D **82**, 034029 (2010).
- [71] J. K. Boomsma and D. Boer, Phys. Rev. D **81**, 074005 (2010).